NATIONAL ADVISORY COMMITTEE FOR AERONAUTICS

TECHNICAL NOTE 4123

ROUGH-WATER IMPACT-LOAD INVESTIGATION OF A CHINE-IMMERSED V-BOTTOM MODEL HAVING A DEAD-RISE ANGLE OF 10°

By Melvin F. Markey and Thomas D. Carpini

Langley Aeronautical Laboratory
Langley Field, Va.

NACA

Washington
October 1957

R

NATIONAL ADVISORY COMMITTEE FOR AERONAUTICS

TECHNICAL NOTE 4123

ROUGH-WATER IMPACT-LOAD INVESTIGATION OF A CHINE-IMMERSED V-BOTTOM MODEL HAVING A DEAD-RISE ANGLE OF 10°

By Melvin F. Markey and Thomas D. Carpini

SUMMARY

A rough-water investigation of a V-bottom chine-immersed model has been made in the Langley impact basin. The model was 20 inches wide and 5 feet long and had a dead-rise angle of 10° and a beam-loading coefficient of 5.78. The impacts occurred on waves ranging from 11 to 60 feet in length and from about 1 to 2 feet in height (length-height ratios from 8.3 to 43.7). The initial flight conditions were held essentially constant. The trim angle was held fixed at 12° with respect to the horizontal, the flight-path angle was about 6°, and the resultant velocity was approximately 65 feet per second. A few planing runs were also made. Time histories of the runs were obtained, and a few typical time histories are presented to show the wave shape, the position of the model on the wave, and the variation of some impact parameters throughout the impact.

The investigation led to the conclusion that the slope of the wave is an important impact parameter. Fairly good agreement between the experiment and an application of smooth-water theory to rough water was obtained for the suitable data.

INTRODUCTION

For the landing-impact problem of the operational seaplane, the rough-water condition is of utmost importance. However, most hydrodynamic impact-load investigations for large-scale models under controlled conditions have been devoted to smooth water because of the relative simplicity of smooth-water testing and the belief that smooth-water landing conditions are fundamental to many rough-water conditions from the standpoint of impact loads. Reference 1, for instance, indicates the existence of a relationship between wave slope and the slope of an equivalent inclined-plane smooth-water surface for a model without chine immersion. However, few tests have been made in rough water for the model with immersed chines, although a few impacts were reported in references 2 and 3. All the impacts in references 1 to 3 were limited to uniform waves from 3 to 6 model lengths.

The need for more extensive data especially for bodies with immersed chines led to the present investigation. The tests were made in irregular waves from 2 to 12 model lengths for one initial set of flight conditions prior to water contact. The model tested had a V-bottom with a dead-rise angle of 10° and a beam-loading coefficient of 5.78. It was tested at a fixed trim of 12° and a resultant velocity of about 65 feet per second. The impacts were made on waves ranging from 1 to 2 feet in height and 11 to 60 feet in length.

This paper presents the data of the investigation in tabular form and as time histories of the loads and motions of the model relative to the wave. In addition, the relation of impact loads to wave slope is shown. In expressing the loads in coefficient form, the waves are considered to be stationary in space. In appendix A other methods of including the wave velocity are considered for the computation of the impact lift coefficient.

SYMBOLS

b	model beam, ft
$C_{L,max}$	maximum impact lift coefficient, $\frac{n_{i,max}W}{\frac{1}{2}\rho V_o^2 b^2}$
C_m	pitching-moment coefficient, $\frac{M_Y}{\frac{1}{2}\rho V_o^2 b^3}$
C_Δ	beam-loading coefficient, $\frac{W}{\rho g b^3}$
g	acceleration due to gravity, 32.2 ft/sec^2
H	wave height measured from trough to crest, ft
L	wave length measured from trough to trough, ft
l	wetted length along model keel, beams
M_Y	pitching moment about stern, lb-ft
n_i	impact-load factor measured normal to undisturbed water surface
t	time after contact, sec

V	resultant velocity of model, ft/sec
V_w	translational velocity of wave, ft/sec
W	dropping weight, 1,670 lb
x_p	horizontal distance from leading center-of-trough point to point on wave coinciding with given particle
x_s	horizontal distance from trough of wave to position of step of model at impact, ft
$\dot{x}$	horizontal velocity of model, ft/sec
$\dot{z}$	vertical velocity of model, ft/sec
γ	flight-path angle relative to undisturbed water surface, deg
θ	slope of wave, deg
ρ	density of water, 1.938 slugs/cu ft
τ	model trim angle relative to undisturbed water surface, deg

Subscripts:

av	average from initial impact to maximum load
e	effective (referred to wave surface)
max	maximum
o	at initial contact
s	at step

APPARATUS

The investigation was conducted in the Langley impact basin with the test equipment described in reference 4. The rough-water conditions required for the tests were generated by the Langley impact-basin wave maker, which is described in reference 1.

Model

The test model was 20 inches wide and had a dead-rise angle of 10° and a prismatic section for a length of 5 feet. The nose of the model was curved upwards to minimize the effects of bow immersions. The plan form and pertinent dimensions of the model are shown in figure 1, and the model attached to the carriage boom at a trim angle of 12° is shown in figure 2.

Instrumentation

Two multichannel oscillographs and an NACA optical wave height recorder were used to obtain the data in this investigation, and record correlation was achieved with standard timing devices connected in circuits that were common to the recorders.

One oscillograph was located on the carriage and was used to record the time histories of the loads and motions of the model. A sample record from this instrument, presented as figure 3, shows the pitching moment, displacement, velocity, and acceleration of the model during three successive impacts. The pitching moment was obtained from a strain-gage dynamometer mounted between the model and the carriage boom. These moments were measured about the front attachment point and transferred to the step of the model. The transfer of the moments led to inaccuracies such that the moment about the step should be considered approximate. Horizontal displacement was measured with the photoelectric pickup described in reference 4, and horizontal velocity was computed from the output of the horizontal displacement recorder and corresponding increments of time. Vertical displacement was measured with an electrical slide wire, while vertical velocity was measured with a small induction-type generator driven by the boom. Vertical accelerations were obtained from two unbonded strain-gage accelerometers, a ±25g accelerometer having a natural frequency of 355 cycles per second and a ±12g accelerometer having a natural frequency of 125 cycles per second.

Wave length was measured with a series of electrical probes mounted perpendicular to the undisturbed water surface along the tank wall and recorded on an oscillograph stationed at the side of the tank. Each probe was positioned just above the water surface and connected to a recording galvanometer in such a way that when a probe became wetted the occurrence was recorded. A wave length was taken as the distance between two given probes that were contacted simultaneously by the corresponding portions of the flanks of two adjoining waves.

Wave height was recorded with an NACA optical wave height recorder which was mounted on the carriage so as to project a light image on the water surface just forward of the model (fig. 4). The image on the water surface was recorded directly by a film drum located so that the rise and

fall of the water surface resulted in a trace moving across the film. This wave height recorder is further described in reference 5.

The position of the model on the wave profile and a measure of the wetted length of the model were obtained with the aid of six water contacts, each an electrical conductor 10 inches long and fabricated into the keel of the model. The principle of operation of these water contacts was similar to that of the probes used to measure wave length.

In general, the results yielded by the instrumentation are believed to be accurate within the following limits:

Horizontal velocity, ft/sec	±0.5
Horizontal distance, x_s, ft	±0.3
Vertical velocity, ft/sec	±0.2
Vertical displacement, ft	±0.02
Acceleration, percent of reading	±5
Time, sec	±0.001
Wave height, in.	±0.4
Wave length, ft	±0.5
Wave slope, deg	±1.0
Wave velocity, ft/sec	±0.5
Weight, lb	±10

PROCEDURE

A series of impacts was made at the Langley impact basin at a fixed trim of 12° and at a beam-loading coefficient of 5.78 (a dropping weight of 1,670 pounds). Most of the impacts were made in rough water, a few impacts being made in smooth water.

The rough-water impacts were made with preset initial flight-path angles of about 6° for the landing impacts and at 0° for the planing impacts. The initial horizontal velocity ranged from about 46 to 61 feet per second for the landing impacts and from about 62 to 66 feet per second for the planing impacts. The vertical velocity for the landing impacts was approximately 6 feet per second. After some of these impacts, the model, which remained rigidly attached to the carriage boom and fixed in trim, entered subsequent waves at reduced vertical velocities. These impacts resulted in data for landing conditions ranging from about $\gamma_o = -3°$ to 5°.

The impacts were made in irregular-shaped waves traveling in a direction opposite to that of the model. A simulated impact of the model in the test area of the impact basin is illustrated in figure 5. The ranges of wave heights and lengths were as follows:

Wave length, ft	Wave height, ft
11 to 15 (1.8 to 2.4 model lengths)	1.08 to 1.57
26 to 33 (4.2 to 5.4 model lengths)	1.20 to 2.05
42 to 60 (6.8 to 9.7 model lengths)	.96 to 1.91

Throughout the landing impacts an upward force of 1 g was applied to the model to simulate wing lift. This force was applied by a buoyancy engine just before initial contact of the model with the water, as described in reference 4.

The planing impacts were made without wing lift. For these runs the model was supported a few inches above the level of the water surface by mechanical catches on the carriage which gripped the boom to which the model was attached. The model was supported in this manner throughout the impacts, the upward movement of the model being resisted only by the 1,670-pound weight of the model and the downward movement being restrained at all positions by gripping the catches.

Several smooth-water impacts were made at initial flight-path angles ranging from 6° to 11°. A wing lift of 1 g was applied throughout these runs, several of which were made under identical test conditions to check the behavior of the test equipment.

RESULTS AND DISCUSSION

The experimental results for this investigation are presented in table I. This table shows that the flight conditions prior to the first impacts were essentially constant; therefore, the results for the first impacts show variations primarily due to different wave conditions. In this paper, the analysis of the results deals essentially with the dependence of maximum impact loads upon such conditions as wave slope and position of impact along the wave. The applicable data are also compared with theory and presented with the theoretical parameters.

Some sample time histories of the loads and motions throughout the impacts are shown in figures 6 to 10. Figures 6 and 7 show impacts with essentially the same initial flight conditions in waves of about 13 feet in length; however, the shape and magnitude of the load curves are different, apparently because of a difference in wave shape. Figures 8 and 9 are time histories for longer waves at about the same initial flight conditions. In figure 8 an impact relatively close to a wave trough is shown with the load buildup typical for this type of impact. The small

value of the slope at contact gives a relatively low initial load and a gradual load buildup. Figure 9 shows an impact with a larger initial slope; in fact, the slope in this case is about the same as the slope at maximum load for the impact of figure 8. In this case, the maximum load is developed very early in the impact and attains a greater magnitude. Figure 10 shows a sample planing run. This run gives an indication of the loads obtained from impacts on the flank of similar waves. A substantial reduction, probably due to the difference in wave shape, may be noted in the load for the second impact.

In order to give an indication of the degree of consistency of the maximum loads developed on waves of about the same length, the maximum impact lift coefficient is plotted against the position of the impact along the wave (fig. 11), where the position of impact x_s is taken as the distance from the trough of the wave to the position of the step of the model at impact. Only the impacts with about the same initial flight conditions are shown. In this figure the maximum lift coefficients appear to be fairly consistent, the position of impact having a more noticeable effect for the short waves. The straight line on these curves which is checked by a few smooth-water points (fig. 11(a), $x_s/L = 0$) represents the value of the maximum lift coefficient as predicted by theory (ref. 6) for smooth-water impacts with initial flight conditions about the same as those for the rough water. The line indicates that the loads in waves are greater than those in smooth water except for impacts near the crest of the wave ($x_s/L = 0.5$). The scatter in figure 11 is believed to be due largely to variations in wave shape for the different impacts. As pointed out previously, although the wave lengths may be of the same magnitude, the actual wave shape may vary considerably. In order to illustrate this variation, figure 12 shows several of the shorter wave profiles with about the same length. The wave shape is seen to vary considerably, although several of the waves also have essentially the same height. The shapes of the longer waves also varied in a similar manner.

It was believed that the wave shape could at least be partially accounted for by using the wave slope as a parameter. The effect of wave slope on the impact lift coefficient is indicated in figure 13. This figure shows the variation of maximum lift coefficient with an average wave slope θ_{av} for the different wave lengths. The circles in figure 13 denote impacts for which the wave slope changed little after water contact ($\theta_o = \theta_{av}$), whereas the squares denote the converse ($\theta_o \neq \theta_{av}$). The three lowest points in figure 13(a) are for the impacts near the crest of the wave where an alleviation of load is expected.

In figure 14, the data of figure 13, excluding the crest impacts, are combined. Figure 14 shows the definite trend of increasing load with increasing wave slope until a flat impact condition is obtained at

$\theta_{av} = 12^{\circ}$. As might be expected, scatter is seen at the flat impact and the load seems to be alleviated as the slope increases further.

The maximum impact loads predicted by the theory of reference 6 are compared with the loads obtained in this investigation. This theory, which is primarily applicable for the smooth-water case of heavily loaded chine-immersed bodies, is applied to the rough-water conditions of this investigation by assuming the wave to be motionless in space and by taking the reference axis along the slope of the wave. The impact is then treated as a smooth-water impact. The flight-path angle used with the theory is simply $\gamma_e = \gamma_o + \theta_{av}$ and the trim is $\tau_e = \tau - \theta_{av}$. This method of calculating load, along with two other methods which incorporate different wave velocities, is presented in more detail in appendix A.

Figure 15 shows the agreement between the theoretical and experimental lift coefficients. The theory was checked for the particular model being tested by a number of smooth-water points and showed good agreement. The rough-water data were then compared with the theoretical data for effective trims equal to or larger than 3°. The agreement is fairly good except for crest impacts where smooth-water theory is not directly applicable.

If all the considered data are plotted against the parameter γ_e as suggested by theory, figure 16 results. In this figure there can be seen a trend similar to that of figure 14; that is, $C_{L,max}$ increases until a value of γ_e is reached at which a flat impact occurs. However, too few data are available to establish the relation between $C_{L,max}$ and the effective trim. Figure 16(b) shows the value of $C_{L,max}$ for the second impacts. Some of these points are higher than those for the first impacts at comparable values of γ_e. These higher values may be partially due to the larger wetted lengths that were usually encountered in the second impacts.

Because the average wave slope θ_{av}, as used in this report, is probably difficult to obtain or estimate in other than controlled test conditions, a relation between the maximum impact lift coefficient and some other function of the wave seemed worthwhile. An attempt at such a relation is made in figure 17, where θ_{av} is approximated by the length and height of the wave by assuming a linear variation such that the value is taken as $\tan^{-1} H/0.5L$. This value is added to the initial flight-path angle and plotted against the maximum lift coefficient. These points give roughly the same average fairing as figure 16, although the scatter is more pronounced.

CONCLUSIONS

A rough-water impact-load investigation of a fixed-trim, V-bottom model with a dead-rise angle of 10° and a beam-loading coefficient of 5.78 in waves from 11 to 60 feet led to the following conclusions:

1. The position of impact along the wave had more effect on the maximum load for the short waves than for the long waves. At the crest of a wave, loads having magnitudes of the same order as smooth-water runs at similar flight conditions were obtained.

2. The maximum impact lift coefficient depends on the local slope of the wave contacted. This slope was considered to be the average slope from initial contact to maximum load.

3. Fairly good agreement between theory and experiment is shown at effective trims of 3° or greater over a range of effective flight-path angles.

Langley Aeronautical Laboratory,
National Advisory Committee for Aeronautics,
Langley Field, Va., July 25, 1957.

APPENDIX A

THREE METHODS FOR COMPUTING MAXIMUM IMPACT LIFT COEFFICIENT $C_{L,max}$ FOR MODEL LANDINGS IN ROUGH WATER

In the present investigation, three methods were considered for computing the impact lift coefficient $C_{L,max}$ for rough-water impacts. The first method involved the initial model velocities and the wave orbital velocities; the second, the initial model velocities and the wave translational velocities; and the third, the initial model velocities only. Each method produced a different resultant velocity for the model and a correspondingly different effective flight-path angle γ_e for the same impact. The effective trim angle τ_e was computed identically for all three methods.

The first method outlined, and the one believed theoretically to be the most nearly correct, is that using the orbital velocity of the wave in conjunction with the initial velocities of the model in determining the resultant velocity. With the assumption that the waves are trochoidal in character, the theoretical orbital velocity V_p is given as

$$V_p = 7.1 \frac{H}{\sqrt{L}} \text{ ft/sec}$$

(see refs. 7 and 8) where H is the wave height (trough to crest) in feet and L is the wave length (trough to trough) in feet.

Since the water particles of a trochoidal wave travel in a circular path, the direction ϕ of a given particle at any point on the wave surface is then taken as

$$\phi = 2\pi \frac{x_p}{L}$$

where x_p is the horizontal distance in feet from the leading center-of-trough point of the wave to the point on the wave coinciding with the particle being considered. During each impact, as a simplification, the water particle whose orbital velocity is used in computing the impact

lift coefficient is taken at the 3/4-wetted-length point of the model bottom at the time of maximum acceleration. Components of the velocity of this particle are added vectorially to the initial model velocities so that the modified resultant velocity yields the following lift coefficient:

$$C_{L,max} = \frac{n_{i,max}W}{\frac{1}{2}\rho V_{o,p}^{2} b^{2}}$$

where $V_{o,p} = \sqrt{\left(\dot{x}_o - V_p \cos \phi\right)^2 + \left(\dot{z}_o + V_p \sin \phi\right)^2}$ as shown by the vector

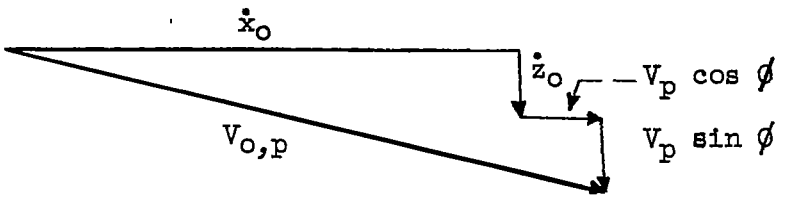

The effective-flight-path angle then becomes

$$\gamma_e = \tan^{-1} \frac{\dot{z}_o + V_p \sin \phi}{\dot{x}_o - V_p \cos \phi} + \theta_{av}$$

where θ_{av} is considered to be the average wave slope along the model from the point of initial contact to that of maximum load.

In the second method, the wave is assumed to be an advancing wedge of water moving toward the test model at the wave velocity V_w. This wave velocity is used together with the initial velocities of the model to compute $C_{L,max}$ as follows:

$$C_{L,max} = \frac{n_{i,max}W}{\frac{1}{2}\rho V_{o,w}^{2} b^{2}}$$

where $V_{o,w} = \sqrt{\left(\dot{x}_o + V_w\right)^2 + \dot{z}_o^2}$ as shown by the vector

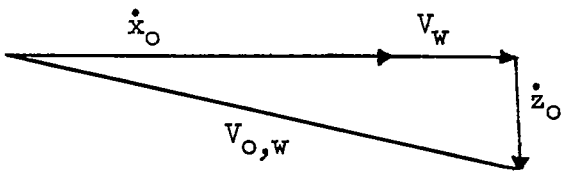

In this case, $\gamma_e = \tan^{-1}\left(\frac{\dot{z}_o}{\dot{x}_o + V_w}\right) + \theta_{av}$.

The final method, which is used in presenting the impact-load data in this report, is the simplest and most direct method in that only the initial velocities of the model are used in obtaining $C_{L,max}$, since the wave was assumed to be motionless. Then,

$$C_{L,max} = \frac{n_{1,max} W}{\frac{1}{2}\rho V_o^2 b^2}$$

where $V_o = \sqrt{\dot{x}_o^2 + \dot{z}_o^2}$ as shown by the vector

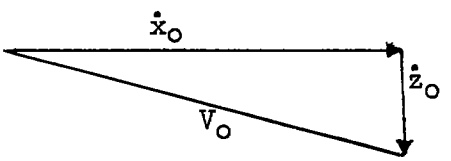

In this case, $\gamma_e = \tan^{-1}\left(\frac{\dot{z}_o}{\dot{x}_o}\right) + \theta_{av}$.

Figure 18 shows comparisons of the impact lift coefficients computed by the various methods. In figure 18 considerable difference is evident between the impact lift coefficients computed by the translating-wave method $\left((C_{L,max})_{trans}\right)$ and the stationary-wave method $\left(C_{L,max}\right)$. Figure 18 shows a smaller difference, generally less than 10 percent, between the impact lift coefficients computed by the orbital-velocity method $\left((C_{L,max})_{orb}\right)$ and the stationary-wave method. The orbital-velocity method is believed to be theoretically the most nearly correct; however, its use involves lengthy computational procedures and rough assumptions in the selection of an effective orbital velocity for each impact. Therefore, the simpler stationary-wave method was used throughout the report in the presentation of the results.

REFERENCES

1. Miller, Robert W.: Hydrodynamic Impact Loads in Rough Water for a Prismatic Float Having an Angle of Dead Rise of 30°. NACA TN 1776, 1948.

2. Batterson, Sidney A.: Water Landing Investigation of a Hydro-Ski Model at Beam Loadings of 18.9 and 4.4. NACA RM L51F27, 1951.

3. Edge, Philip M., Jr.: Impact-Loads Investigation of Chine-Immersed Models Having Concave-Convex Transverse Shape and Straight or Curved Keel Lines. NACA TN 3940, 1957.

4. Batterson, Sidney A.: The NACA Impact Basin and Water Landing Tests of a Float Model at Various Velocities and Weights. NACA Rep. 795, 1944. (Supersedes NACA WR L-163.)

5. Edge, Philip M., Jr.: Instrumentation for Investigation of Seaplane Impact Loads in Waves. Proc. First Conf. on Coastal Eng. Instruments (Berkeley, Calif., Oct. 31 - Nov. 2, 1955), Council on Wave Res., The Eng. Foundation, 1956, pp. 213-226.

6. Schnitzer, Emanuel: Theory and Procedure for Determining Loads and Motions in Chine-Immersed Hydrodynamic Impacts of Prismatic Bodies. NACA Rep. 1152, 1953. (Supersedes NACA TN 2813.)

7. Hedrick, I. G., and Siebert, E. G.: Water Loads Investigation - Airplane Model XJR2F-1. Rep. No. 2903.41, Grumman Aircraft Eng. Corp., May 19, 1946.

8. Lamb, Horace: Hydrodynamics. Sixth ed., Cambridge Univ. Press, 1932, pp. 363-475.

TABLE I.- IMPACT LOADS AND WAVE DATA FROM ROUGH-WATER TESTS OF A CHINE-IMMERSED 10° DEAD-RISE MODEL AT $\tau = 12°$

Run	Impact	At contact -					At $n_{1,max}$ -					Wave conditions				
		h, ft/sec	$\dot{z}$, ft/sec	x_s, ft	γ, deg	t, sec	n_1	$C_{L,max}$	M_Y, lb-ft	C_m	l, beams	θ_o, deg	θ_{av}, deg	L, ft	H, ft	V_w, ft/sec
Rough-water impact																
1	1	6.10	46.29	18.0	7.51	0.038	1.3	0.37	1,400	0.15	0.50	0	0	42	0.96	13.00
2	1	5.75	60.98	15.6	5.39	.036	2.4	.40	4,700	.28	1.30	3	3	44	1.09	13.00
3	1	6.10	59.30	13.0	6.00	.007	6.8	1.20	15,300	.96	1.10	11	7	33	1.20	12.45
4	1	6.20	60.15	5.2	5.88	.037	4.9	.84	21,400	1.30	3.10	2	7	33	1.69	13.39
5	1	6.03	59.88	1.7	5.90	.020	8.3	1.42	25,200	1.43	3.50	12	12	26	1.67	10.81
6	1	6.40	60.91	9.7	6.00	.027	6.5	1.08	13,900	.85	1.65	12	7	33	1.32	13.25
7	1	5.80	61.16	8.0	5.30	.013	7.3	1.20	16,900	1.00	2.35	10	10	26	1.74	11.00
8	1	6.30	59.32	8.3	6.00	.016	7.5	1.30	19,300	1.21	2.90	7	10	27	1.79	11.20
9	1	5.30	59.88	3.6	5.23	.014	8.4	1.45	13,700	.85	2.75	12	12	27	1.64	10.72
10	1	5.63	59.88	10.4	5.39	.005	9.9	1.70	15,800	.98	2.50	12	12	27	1.61	11.19
11	1	5.70	60.06	6.4	5.25	.004	4.4	.74	6,900	.43	.50	12	12	15	1.27	8.51
11	2	5.80	58.48	2.5	5.80	.005	10.4	1.89	16,000	.80	2.75	12	12	15	1.27	8.51
11	3	-.75	58.54	2.3	-.74	.004	6.9	1.26	16,200	1.07	2.50	12	12	14	1.27	8.51
12	1	5.65	60.24	5.4	5.00	.005	9.3	1.58	16,300	1.00	1.00	15	15	14	1.22	8.88
12	2	2.75	59.88	3.6	2.63	.005	10.0	1.72	23,300	1.45	2.10	15	15	14	1.22	8.88
12	3	-1.50	59.26	4.2	-1.45	.005	5.7	1.02	15,100	.96	1.75	12	12	14	1.22	8.88
13	1	5.94	60.61	4.3	5.30	.005	10.4	1.74	27,600	1.67	2.00	17	14	14	1.38	9.25
13	2	.96	60.24	4.3	.92	.006	5.4	.92	13,000	.80	2.00	12	12	15	1.08	9.25
13	3	-2.59	59.52	5.2	-2.50	.010	1.8	.31	4,500	.28	.75	18	15	14	1.38	9.25
14	1	5.56	59.17	3.4	5.37	.006	8.1	1.42	22,000	1.39	1.20	12	12	12	1.57	8.28
14	2	2.38	60.24	2.2	2.18	.017	8.8	1.51	47,000	2.84	1.75	21	21	14	1.57	8.28
14	3	-1.88	59.52	3.9	-1.84	.005	2.6	.46	200	.01	1.00	12	12	13	1.12	8.28
15	1	5.53	60.61	3.6	5.30	.005	10.6	1.78	27,100	1.64	2.00	12	12	14	1.35	8.60
15	2	1.07	59.17	2.4	1.00	.007	9.8	1.74	40,200	2.57	3.05	15	14	15	1.35	8.60
15	3	-2.23	58.14	4.7	-2.20	.005	1.7	.31	3,000	.21	1.50	12	15	14	1.35	8.60
16	1	5.85	60.24	4.4	5.57	.003	7.6	1.29	8,700	.53	1.30	12	12	14	1.44	8.23
16	2	3.15	59.52	1.7	3.00	.013	6.6	1.15	30,000	1.88	2.75	18	17	13	1.44	8.23
16	3	-.86	59.48	4.0	-.84	.008	7.0	1.23	19,000	1.20	1.90	17	17	13	1.44	8.23
17	1	6.24	59.52	4.1	6.00	.004	8.2	1.41	15,100	.94	1.35	12	12	12	1.35	8.16
17	2	3.76	59.52	1.5	3.62	.011	6.9	1.21	31,400	1.98	3.10	14	15	14	1.35	8.16
17	3	-1.02	59.88	2.2	-1.00	.016	3.0	.55	14,300	1.21	1.45	24	18	13	1.35	8.16
18	1	5.99	59.52	2.7	5.80	.004	11.2	1.94	28,100	1.75	2.00	16	12	11	1.16	7.80
18	2	.86	59.17	.8	.84	.011	9.0	1.59	37,700	2.41	3.10	20	13	11	1.16	7.80
18	3	-2.89	57.80	2.9	-2.82	.008	2.5	.46	5,300	.35	1.00	12	16	11	1.16	7.80
19	1	5.89	58.82	3.5	5.80	.006	8.0	1.42	9,500	.61	1.25	12	17	11	1.24	7.71
19	2	3.25	58.82	1.4	3.17	.018	7.3	1.30	29,400	1.90	2.50	12	17	11	1.24	7.71
19	3	-.71	58.14	1.2	-.70	.010	4.0	.73	10,300	.68	2.35	20	16	12	1.24	7.71
20	1	6.34	59.52	3.2	6.00	.004	6.2	1.07	8,100	.52	1.00	23	23	10	1.35	8.46
20	2	4.82	59.52	1.9	4.66	.006	9.3	1.61	26,500	1.66	2.25	12	16	11	1.35	8.46
20	3	.00	58.82	10.3	.00	.023	3.3	.60	14,700	.94	3.30	24	14	10	1.35	8.46
20	4	-2.74	58.14	3.2	-2.67	.007	2.6	.47	5,000	.33	2.00	16	14	11	1.35	8.46
21	1	6.65	60.24	5.1	6.25	.010	1.6	.28	1,200	.08	1.20	8	8	12	1.15	7.65
21	2	5.18	59.88	1.3	5.00	.006	10.4	1.78	26,700	1.65	2.80	20	16	11	1.23	7.65
21	3	-2.00	59.88	2.1	-2.00	.006	3.6	.61	6,700	.42	2.50	12	12	12	1.15	7.65
22	1	6.54	59.52	4.5	6.25	.004	9.1	1.56	13,000	.81	1.50	12	12	12	1.23	7.31
22	2	3.30	58.82	1.2	3.20	.009	9.9	1.77	34,400	2.26	2.30	14	15	11	1.12	7.31
22	3	-1.07	58.14	1.8	-1.00	.010	5.4	1.00	19,000	1.27	2.00	14	18	12	1.12	7.31
23	1	6.30	60.98	3.5	6.00	.006	4.1	.68	4,700	.28	1.10	12	17	10	1.12	7.86
23	2	4.92	60.61	2.9	4.67	.005	11.1	1.86	23,700	1.42	2.75	12	12	14	1.27	7.86
23	3	-.56	58.82	.9	-.50	.005	9.5	1.69	30,400	1.97	3.00	12	13	12	1.08	7.86
23	4	-3.25	58.50	.4	-3.18	.006	4.8	.86	9,600	.63	1.50	18	18	12	1.27	7.86
24	1	5.74	59.32	15.3	5.32	.006	5.5	.96	10,200	.64	.75	6	6	49	1.42	13.75
25	1	6.14	58.82	18.6	6.00	.006	6.1	1.09	3,500	.23	1.20	7	7	49	1.68	13.31
26	1	6.55	58.82	18.2	6.48	.007	5.7	1.00	6,500	.41	1.30	8	8	49	1.56	13.19
27	1	6.09	59.52	.9.9	5.80	.085	4.5	.79	19,600	1.23	2.60	0	5	54	1.57	13.78
28	1	6.40	60.98	18.3	6.00	.011	3.5	.58	5,600	.33	1.10	5	5	54	1.91	14.15
29	1	6.24	59.52	27.4	6.00	.020	1.4	.24	900	.06	.45	0	0	54	1.82	14.09
30	1	5.89	60.00	4.4	5.66	.042	3.8	.62	8,700	.52	1.35	0	5	56	1.83	14.00
31	1	6.40	59.52	13.0	6.17	.055	4.4	.77	18,800	1.18	3.50	4	7	52	1.70	13.91
Rough-water planing																
32	1	-0.10	64.94	27.0	-0.10	0.037	1.6	0.24			1.50	5	5	56	1.81	13.99
33	1	.00	65.79	23.8	.00	.006	1.9	.28			1.25	5	5	58	1.67	14.26
34	1	.10	65.79	3.2	.10	.030	1.7	.25			1.00	6	6	60	1.80	15.00
35	1	.00	65.79	11.2	.00	.005	3.9	.57			1.60	9	9	29	1.86	11.72
35	2	-.10	62.50	10.0	-.10	.007	2.4	.38			1.00	8	8	29	2.05	11.72
35	3	-.10	63.29	11.2	-.10	.006	1.7	.26			1.10	7	7	29	1.92	11.72
36	1	-.10	66.67	9.5	-.10	.004	7.1	.99			1.20	12	13	28	1.92	11.57
36	2	-.10	66.44	10.9	-.10	.004	3.0	.39			1.10	12	10	28	1.90	11.57
36	3	-.15	62.50	12.2	-.14	.003	2.4	.38			1.35	10	10	28	2.02	11.57
37	1	-.20	65.79	4.0	-.30	.003	3.8	.53			1.20	16	12	12	1.27	7.37
37	2	-.10	64.10	4.5	-.10	.005	1.9	.29			.85	9	9	12	1.14	7.37
37	3	.00	64.94	3.7	.00	.004	3.5	.52			1.15	12	12	12	1.33	7.37
37	4	-.05	63.29	3.7	-.05	.006	4.0	.62			1.20	16	13	12	1.29	7.37
37	5	.20	64.10	3.9	.30	.006	5.8	.87			1.50	13	13	12	1.32	7.37
37	6	.10	64.10	3.7	.10	.007	5.5	.83			1.35	16	13	12	1.31	7.37
Smooth-water impact																
38	1	9.85	52.63		10.60	0.050	2.4	0.52	3,700	0.29	1.40					
39	1	10.10	52.63		10.86	.052	2.4	.52	4,000	.31	1.40					
40	1	10.15	52.60		10.92	.050	2.4	.51	4,000	.31	1.50					
41	1	9.15	53.33		9.74	.052	2.2	.46	3,400	.26	1.60					
42	1	8.85	53.91		9.32	.050	2.2	.47	3,500	.28	1.50					
43	1	8.93	52.36		9.68	.050	2.1	.47	3,400	.27	1.30					
44	1	5.68	52.63		6.16	.070	1.3	.29	1,900	.15	1.65					
45	1	5.84	58.48		5.70	.065	1.6	.28	2,100	.15	1.25					

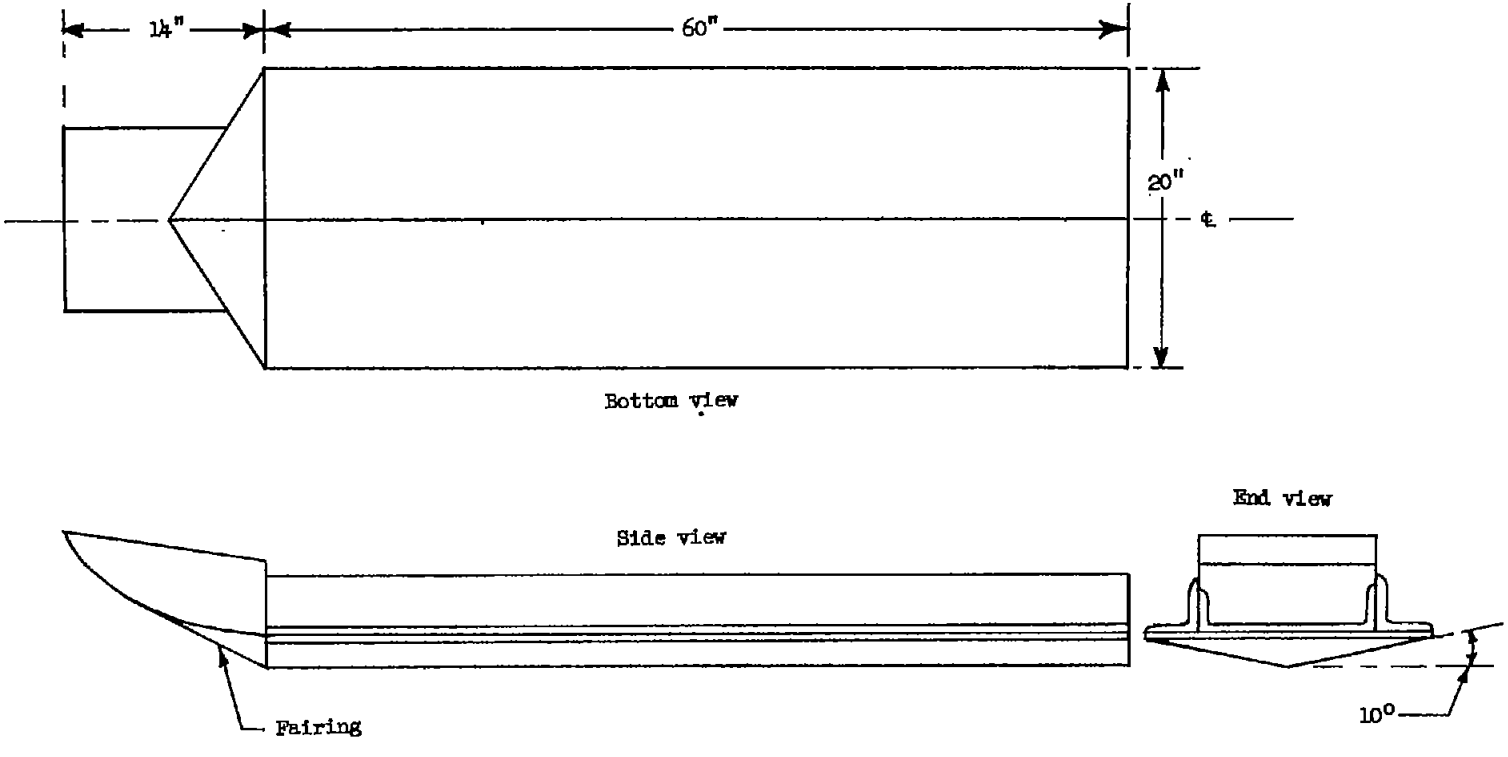

Figure 1.- Plan form and dimensions of 10° dead-rise V-bottom model.

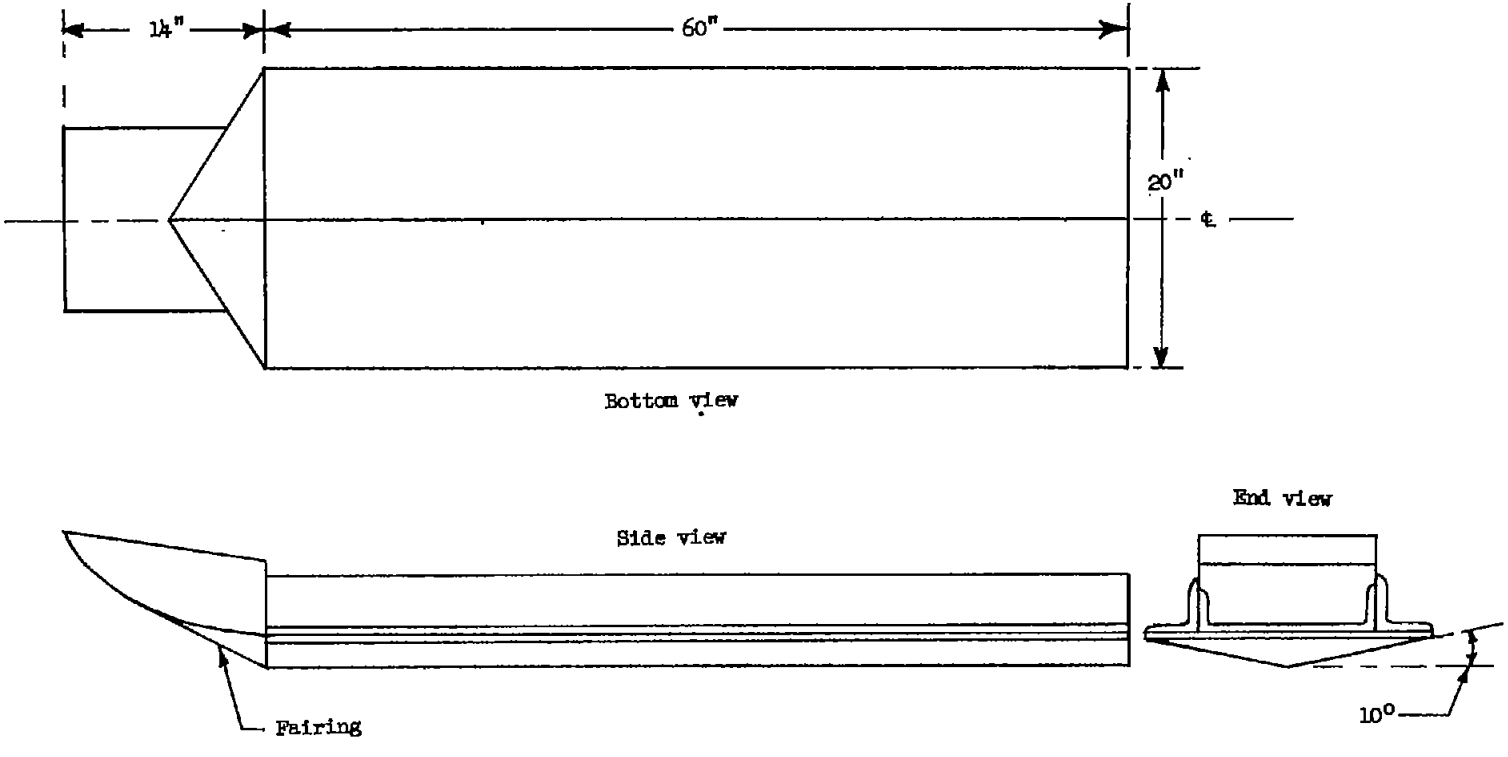

Figure 1.- Plan form and dimensions of 10° dead-rise V-bottom model.

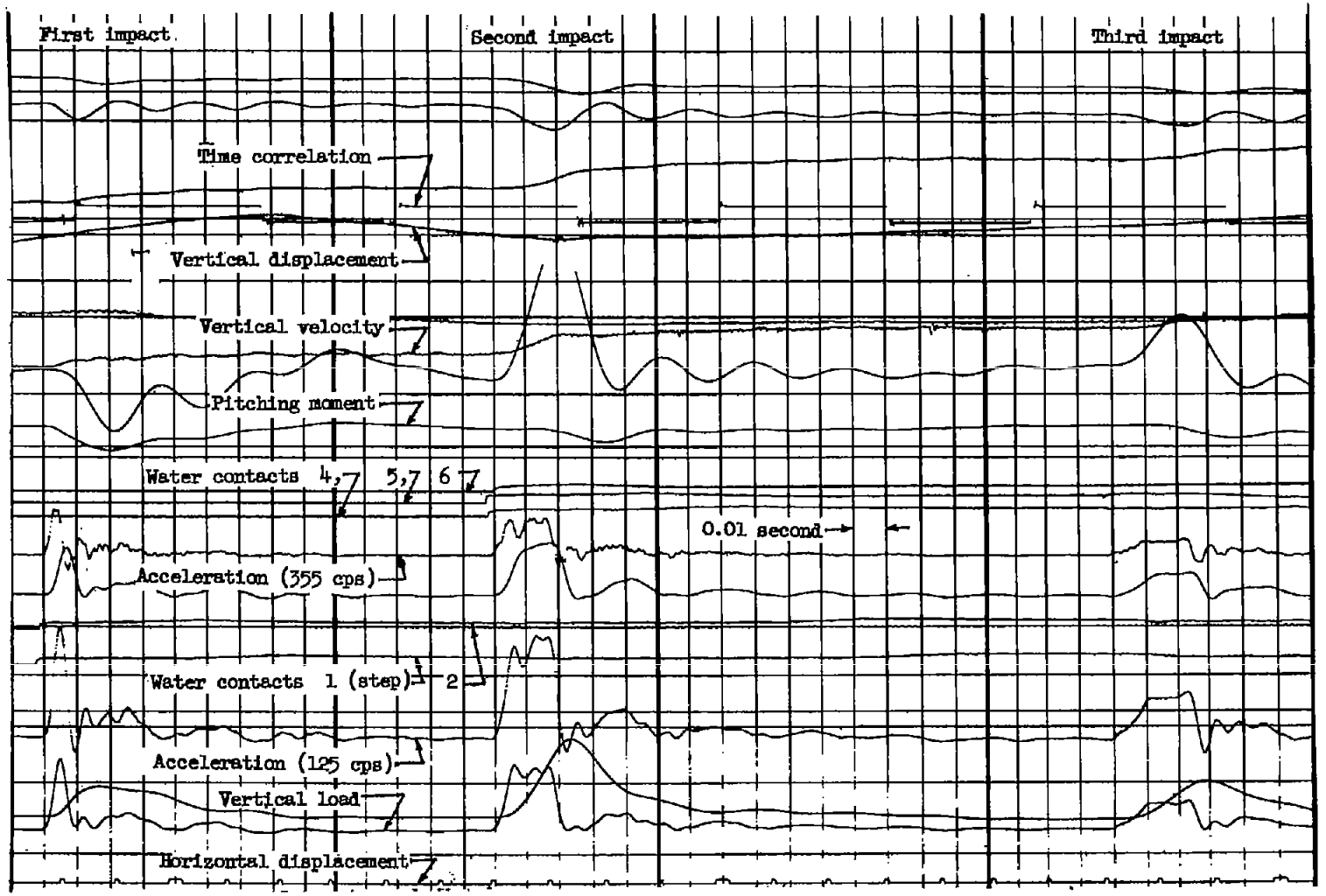

Figure 3.- Sample oscillograph record showing time histories for run 17.

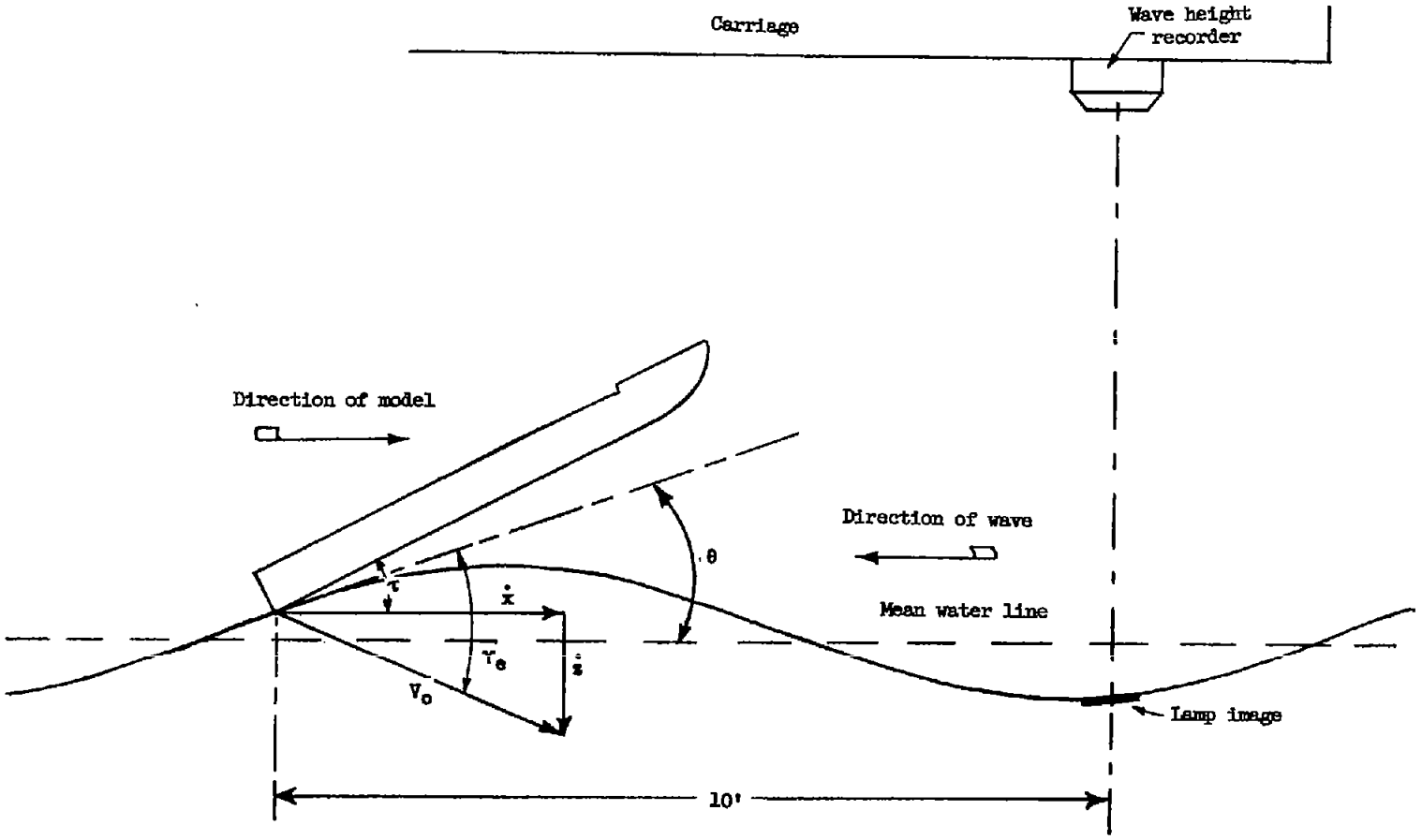

Figure 4.- Geometric relations at contact.

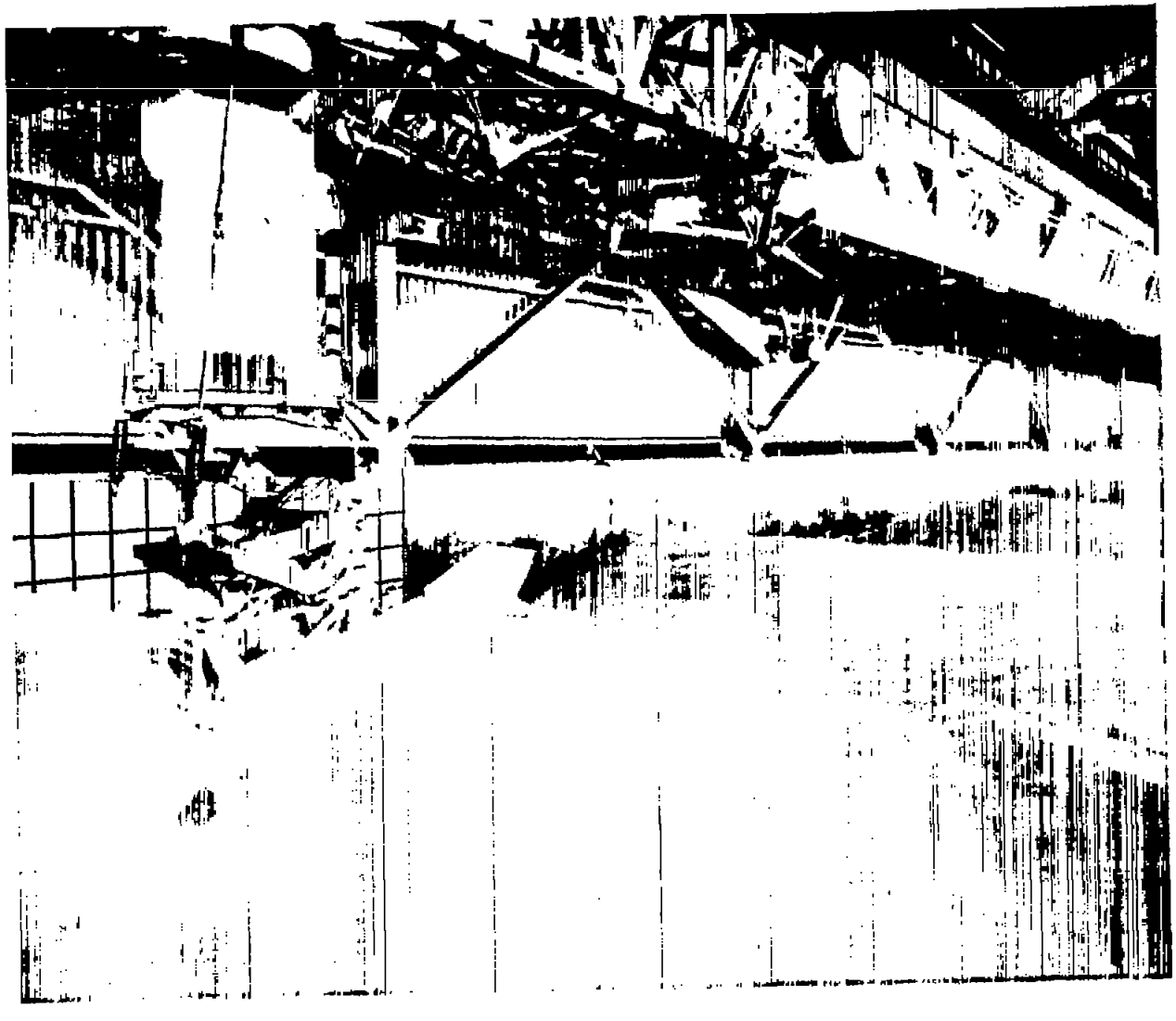

Figure 5.- Photograph of test setup. L-91389

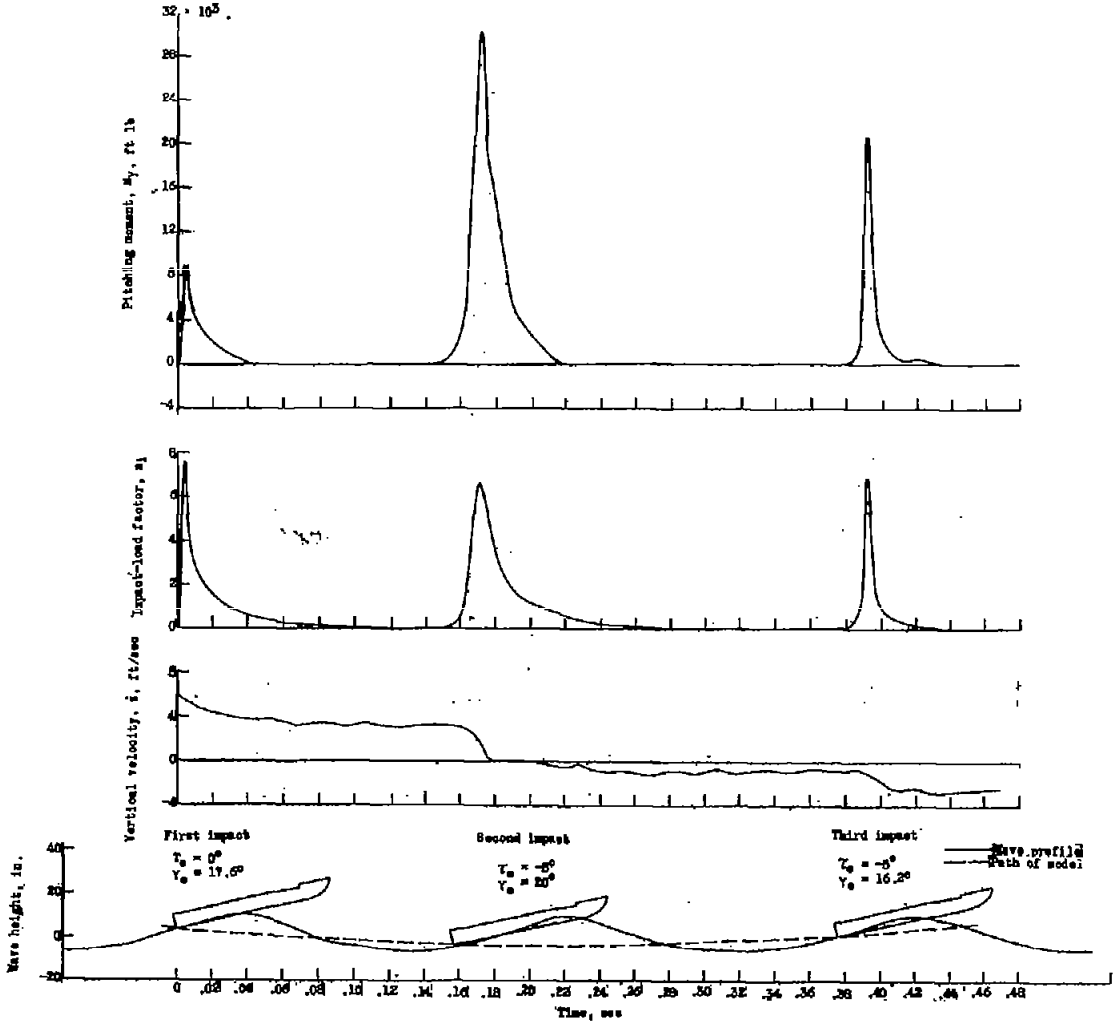

Figure 6.- Time histories of loads and motions experienced during run 16. Wave lengths, 14, 13, and 13 feet; $\dot{x}$ = 60 feet per second.

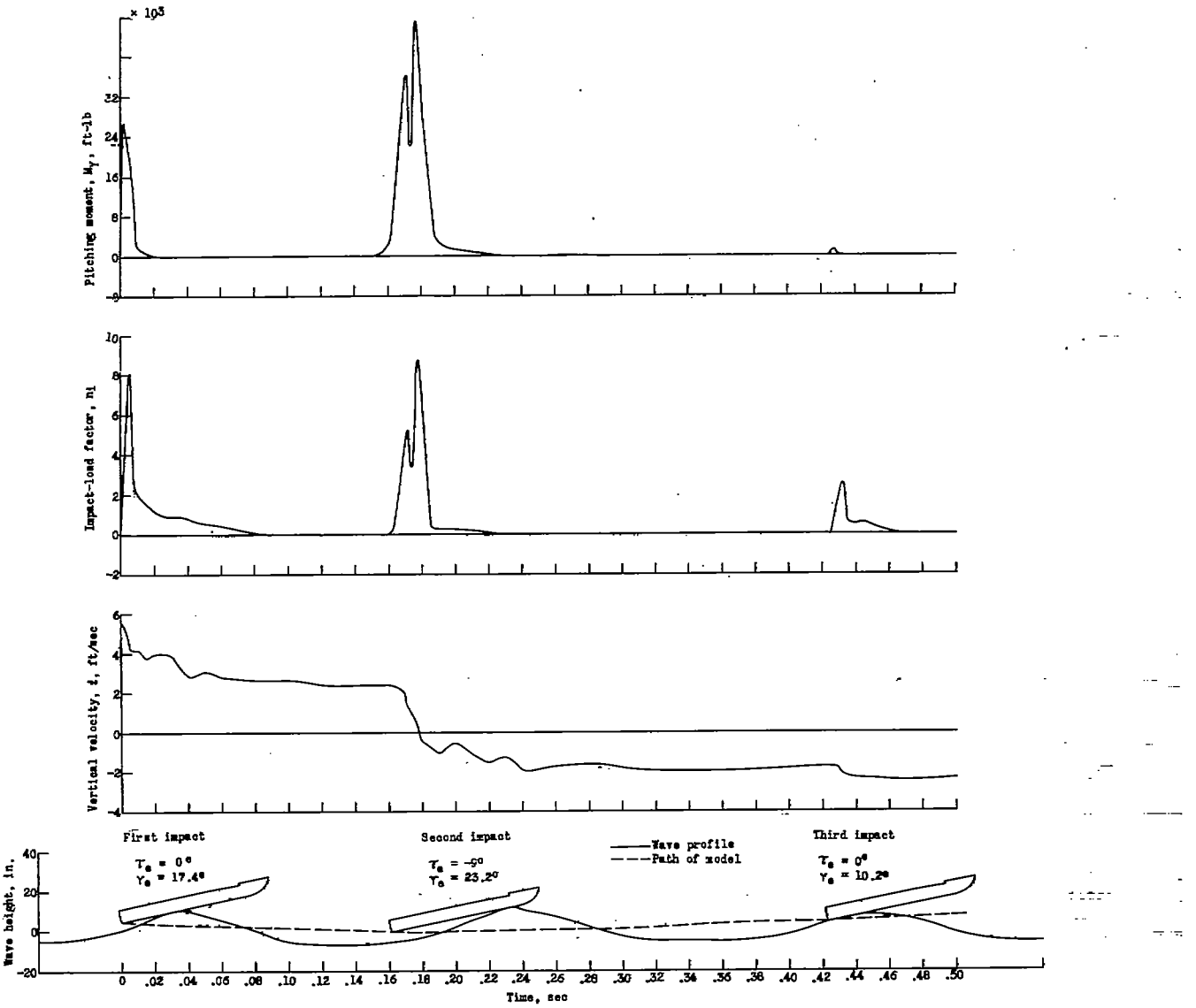

Figure 7.- Time histories of loads and motions experienced during run 14. Wave lengths, 12, 14, and 13 feet; $\dot{x}$ = 60 feet per second.

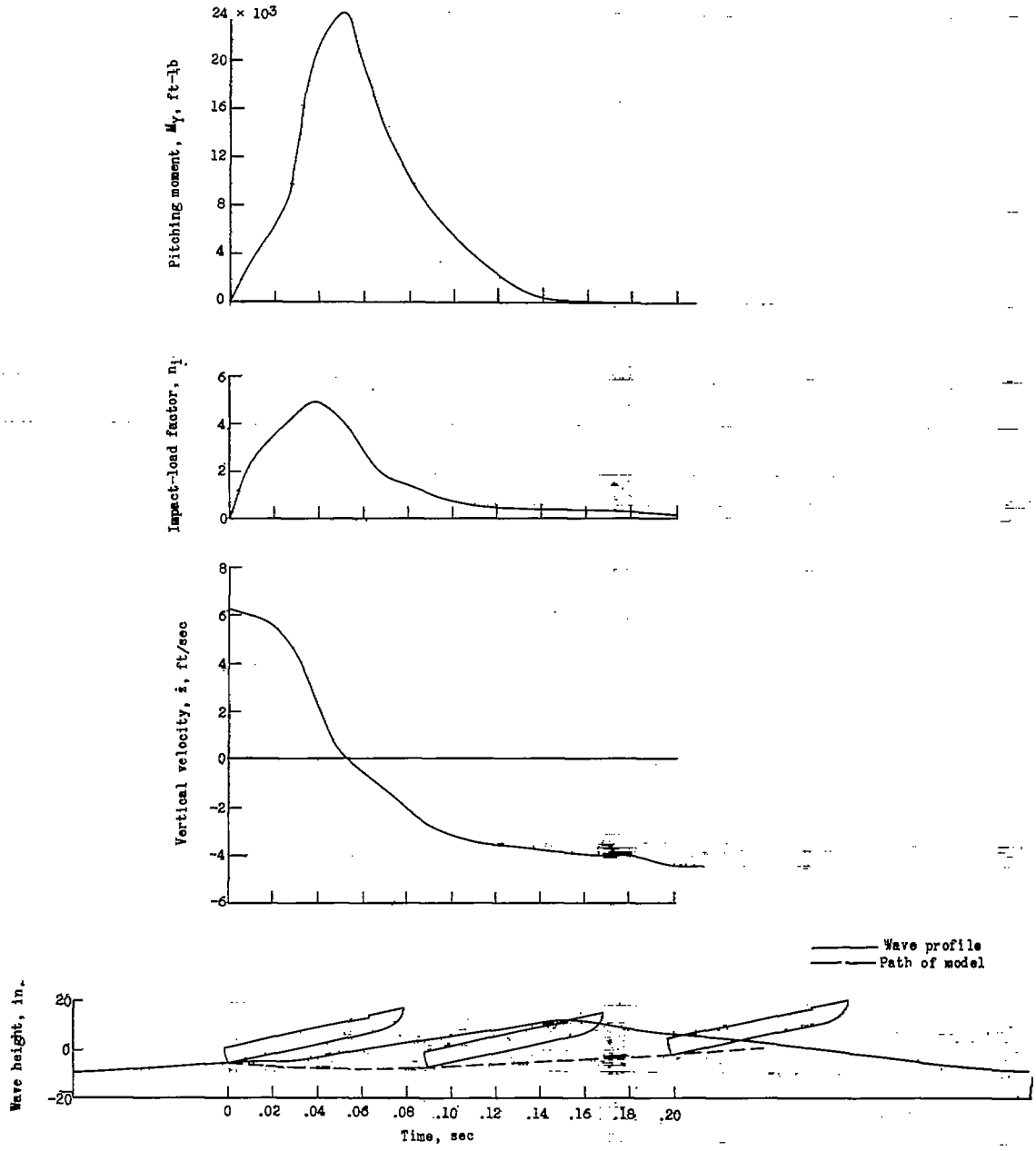

Figure 8.- Time histories of loads and motions experienced during run 4. $\tau_e = 5^\circ$; $\gamma_e = 12.9^\circ$; wave length, 33.0 feet; $\dot{x} = 60$ feet per second.

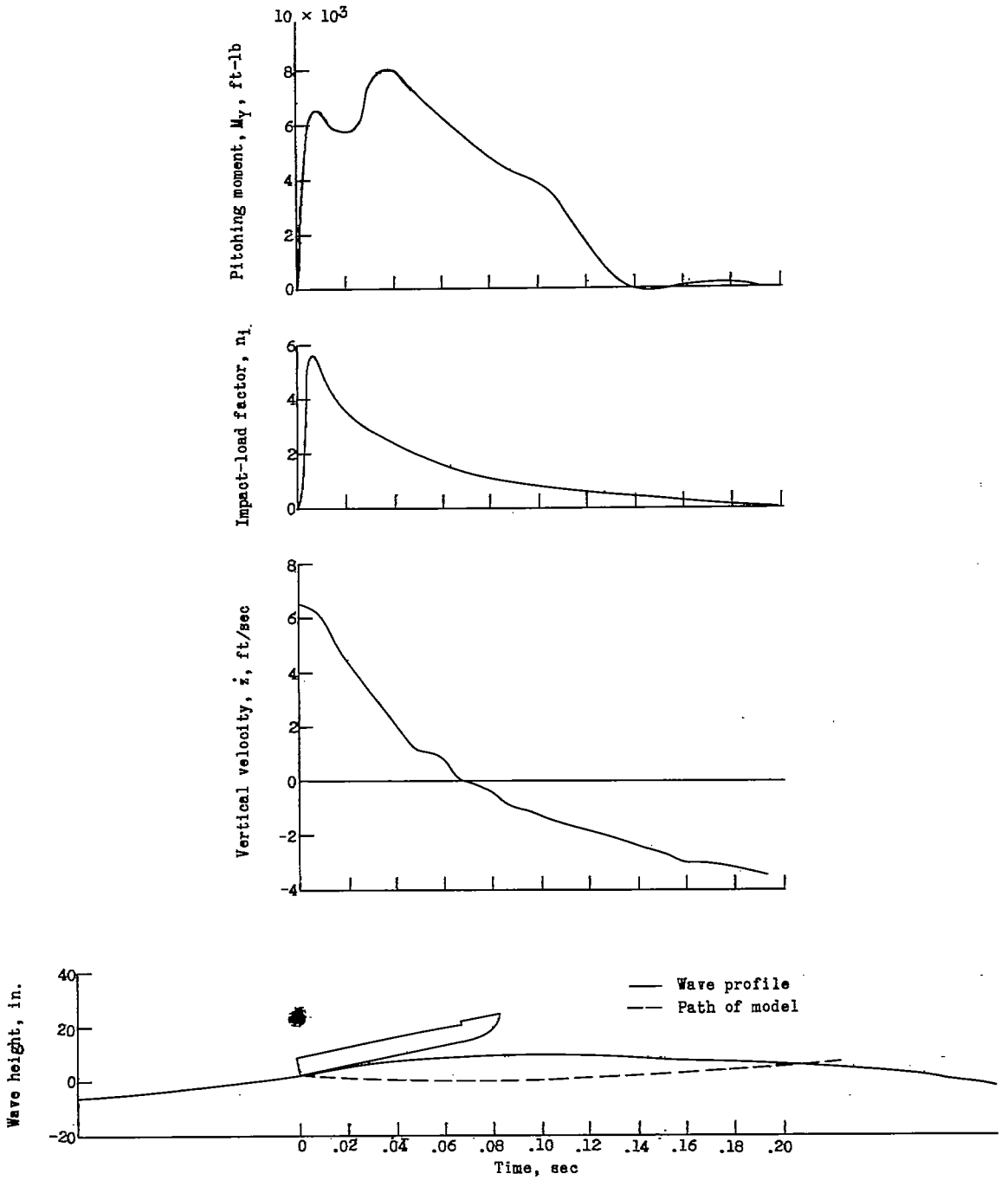

Figure 9.- Time histories of loads and motions experienced during run 26. $\tau_e = 4^\circ$; $\gamma_e = 14.5^\circ$; wave length, 49 feet; $\dot{x} = 59$ feet per second.

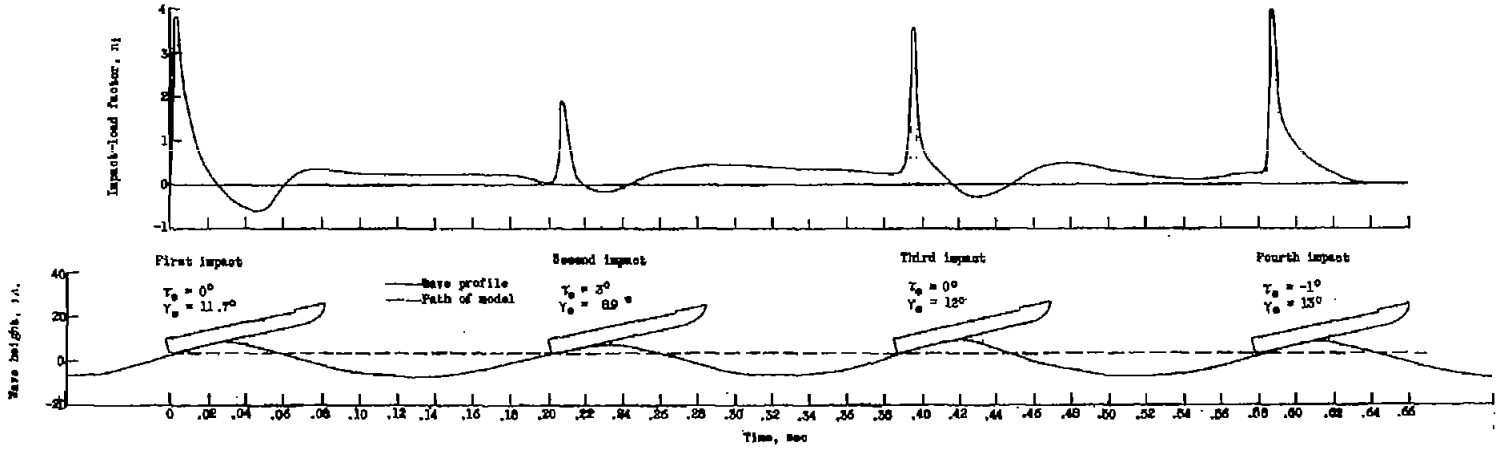

Figure 10.- Time histories of loads and motions experienced during run 37. Wave length, 12 feet; $\dot{x}$ = 66 feet per second.

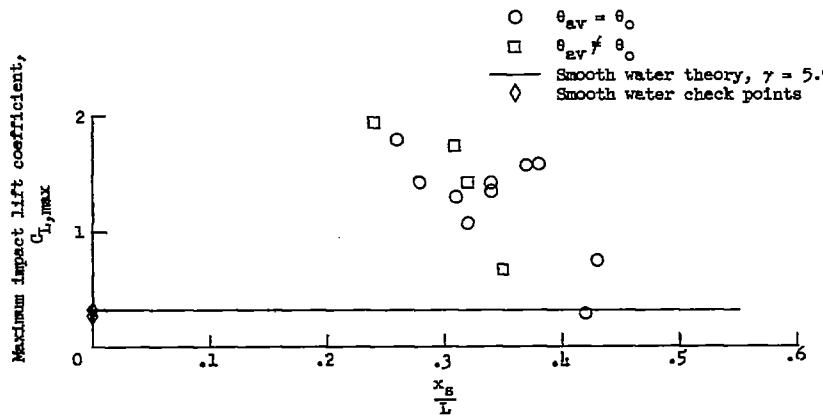

(a) $\gamma_o = 5.0^\circ$ to 6.3°; L = 11 to 15 feet; H = 1.12 to 1.57 feet.

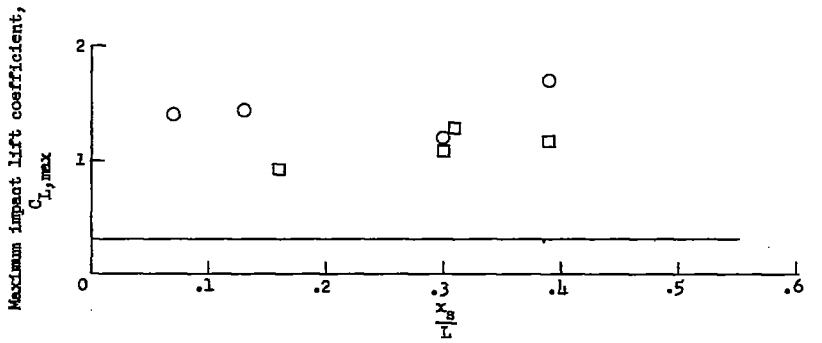

(b) $\gamma_o = 5.3^\circ$ to 6.0°; L = 26 to 33 feet; H = 1.20 to 1.79 feet.

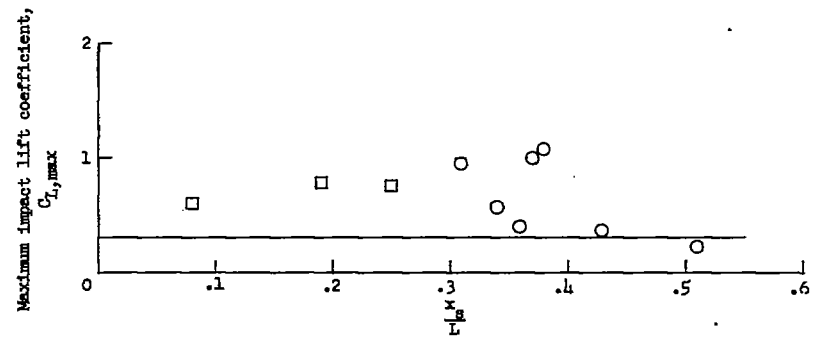

(c) $\gamma_o = 5.3^\circ$ to 7.5°; L = 42 to 56 feet; H = 0.96 to 1.91 feet.

Figure 11.- Variation of maximum impact lift coefficient with position of impact along wave.

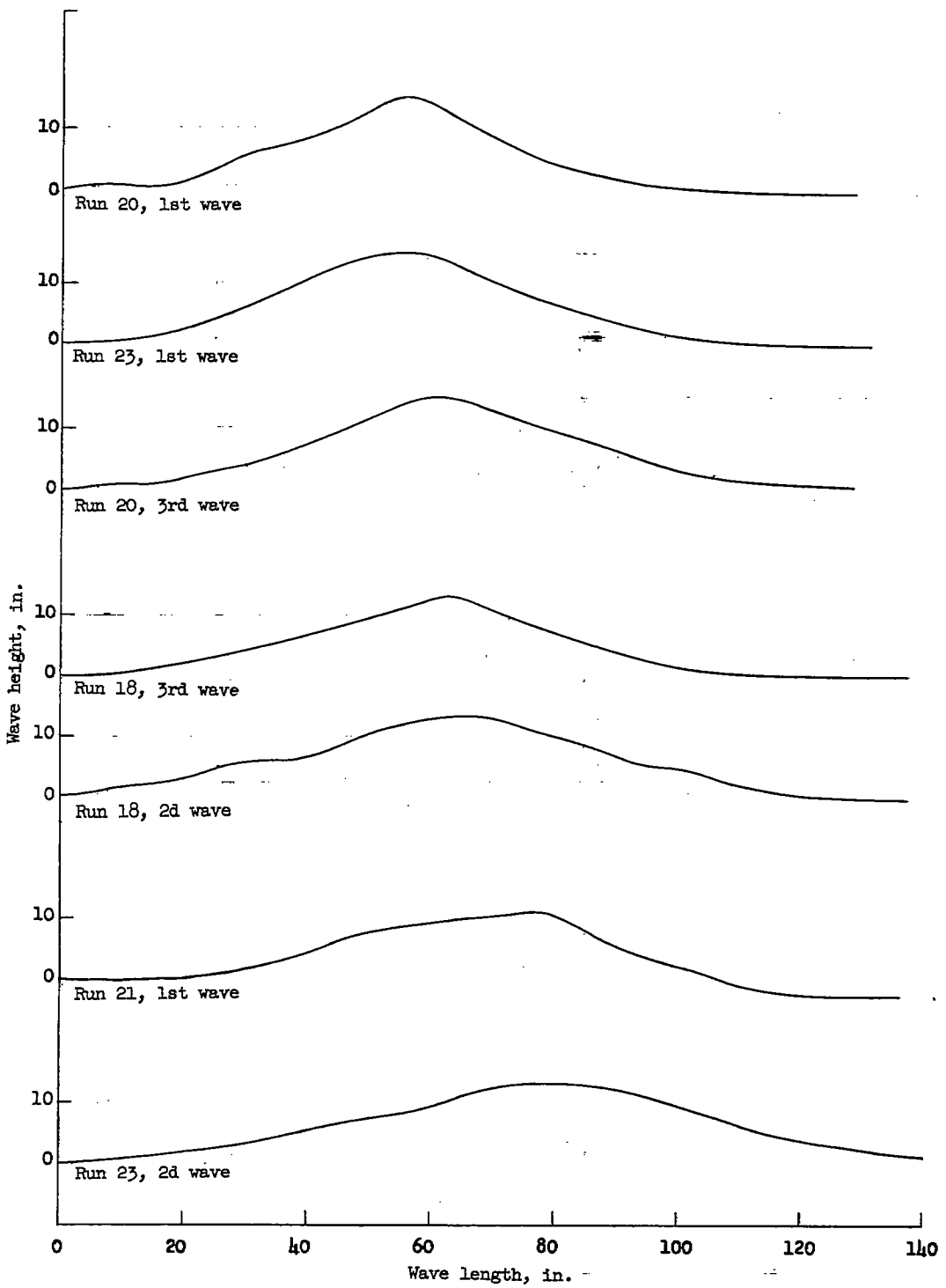

Figure 12.- Some wave profiles for shorter waves.

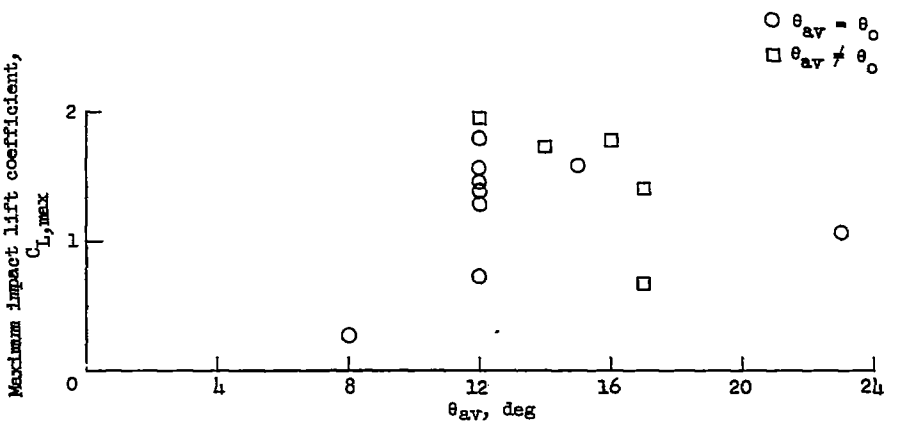

(a) γ_o = 5.0° to 6.3°; L = 11 to 15 feet; H = 1.12 to 1.57 feet.

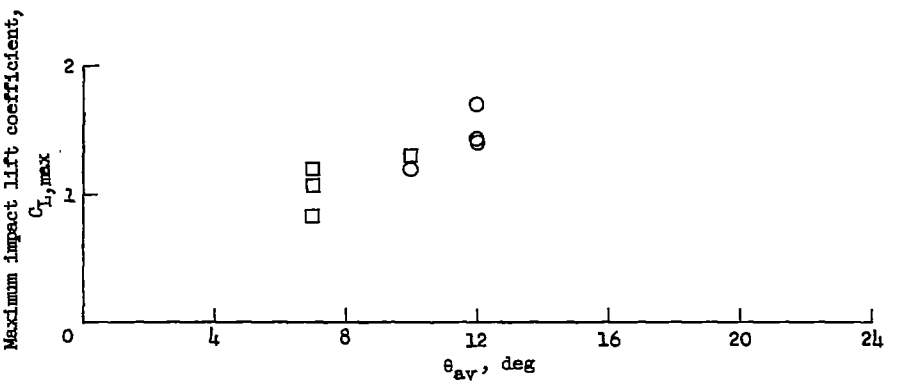

(b) γ_o = 5.3° to 6.0°; L = 26 to 33 feet; H = 1.20 to 1.79 feet.

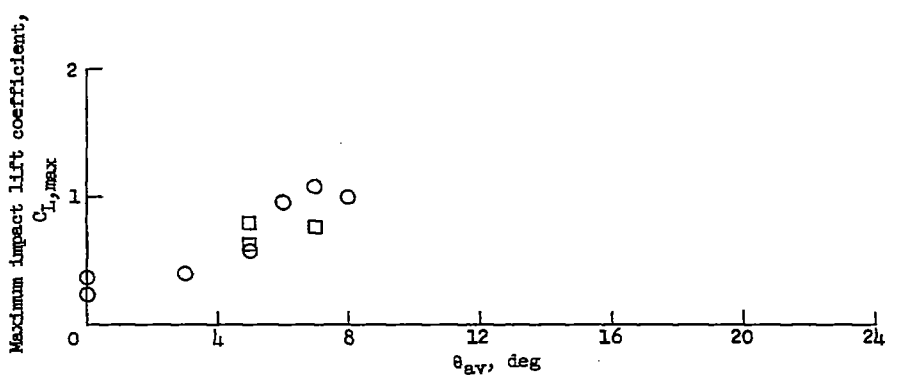

(c) γ_o = 5.3° to 7.5°; L = 44 to 56 feet; H = 0.96 to 1.91 feet.

Figure 13.- Variation of maximum impact lift coefficient with the average slope of the wave from contact to maximum load for various length waves.

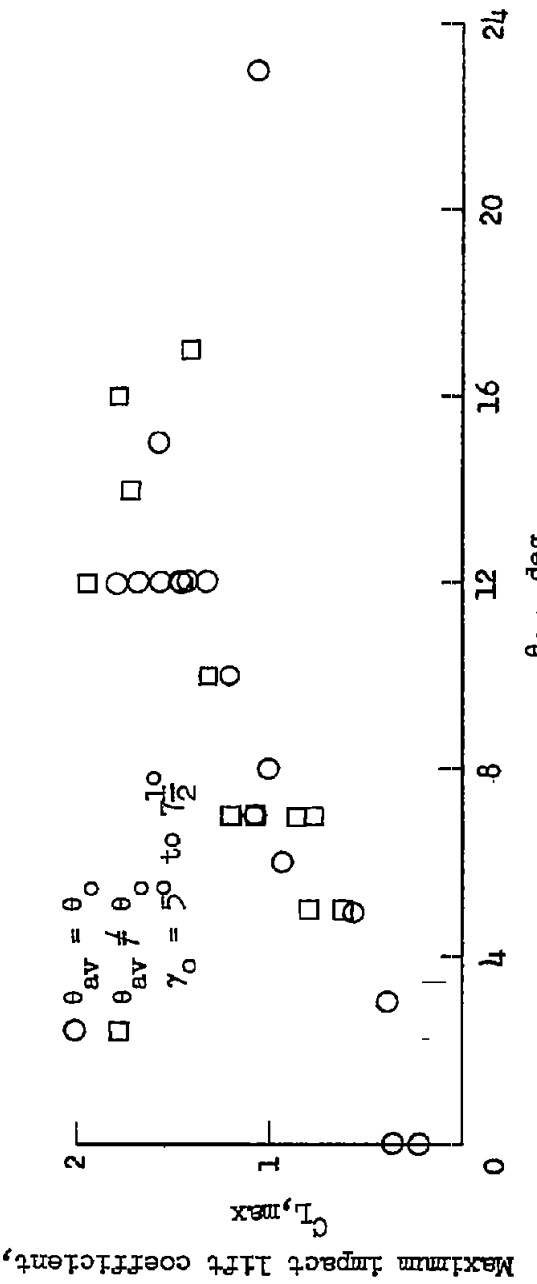

Figure 14.- Variation of maximum impact lift coefficient with average slope of wave from initial contact to maximum load for all waves.

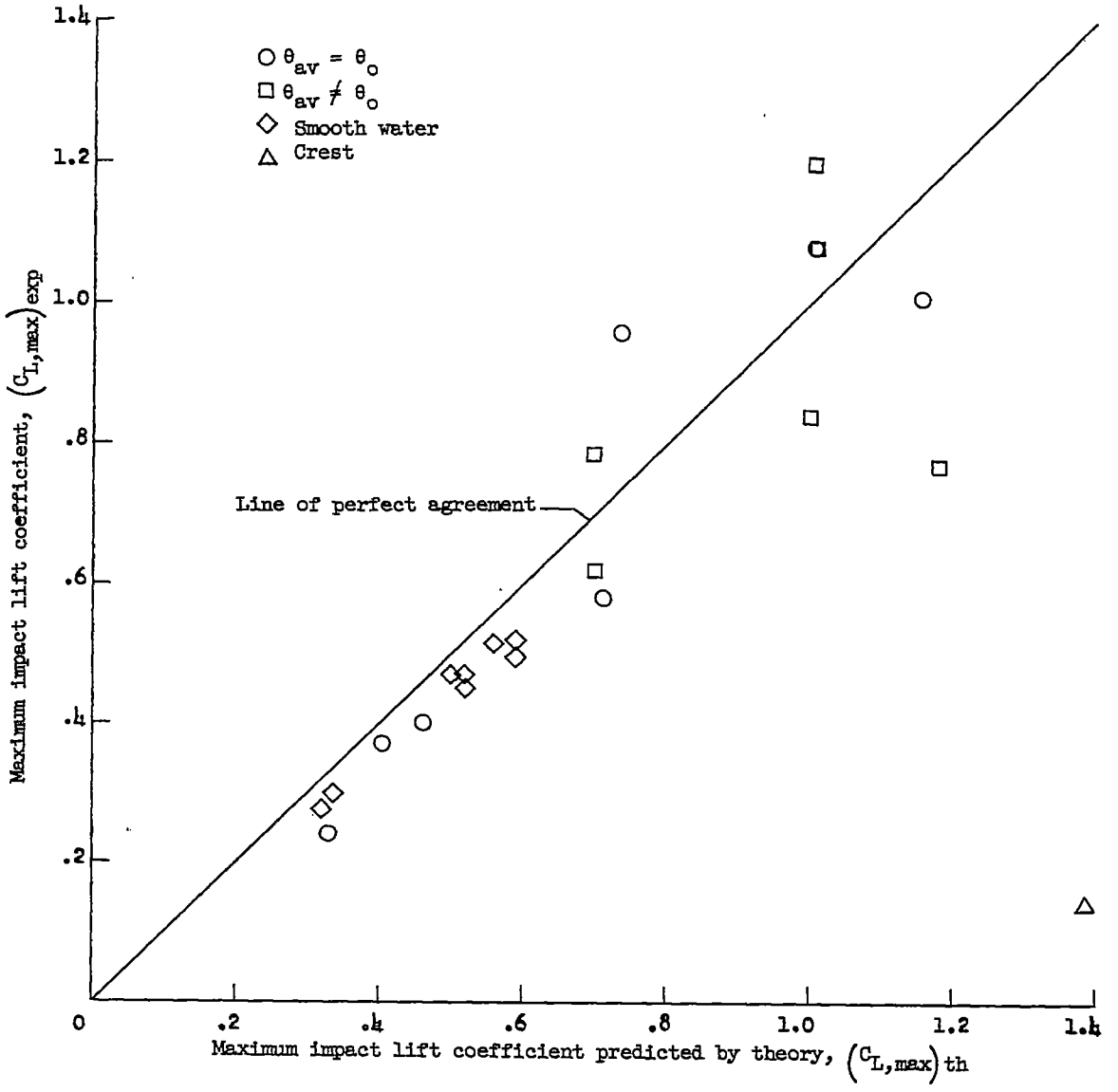

Figure 15.- Comparison of experimental and theoretical maximum load coefficients.

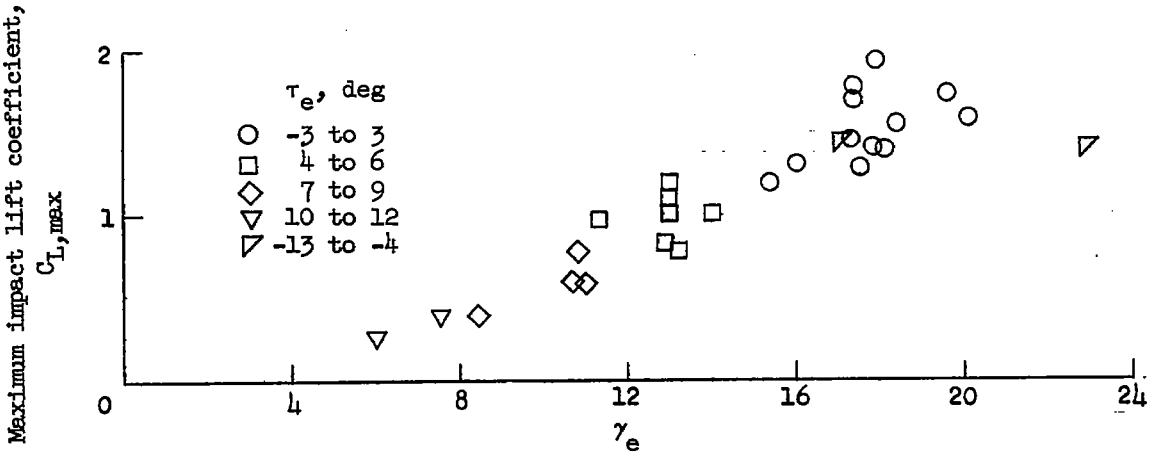

(a) First impacts.

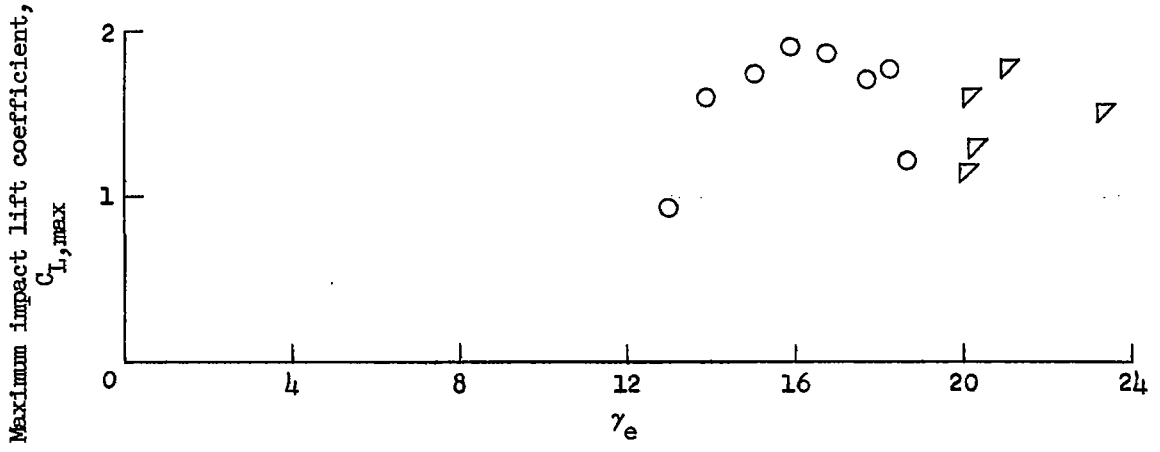

(b) Second impacts.

Figure 16.- Variation of maximum impact lift coefficient with effective flight-path angle.

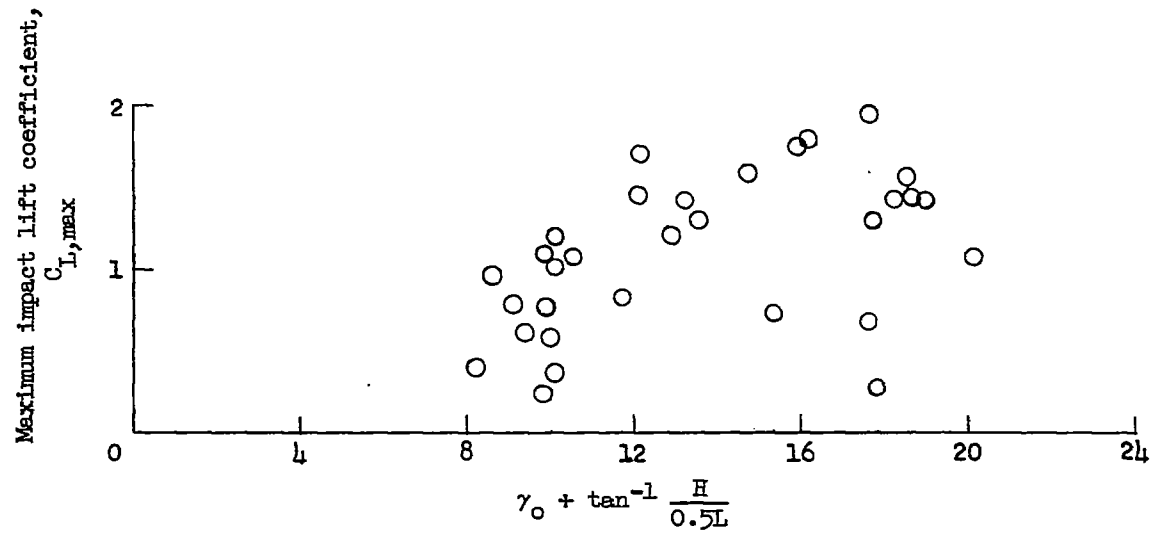

(a) First impacts.

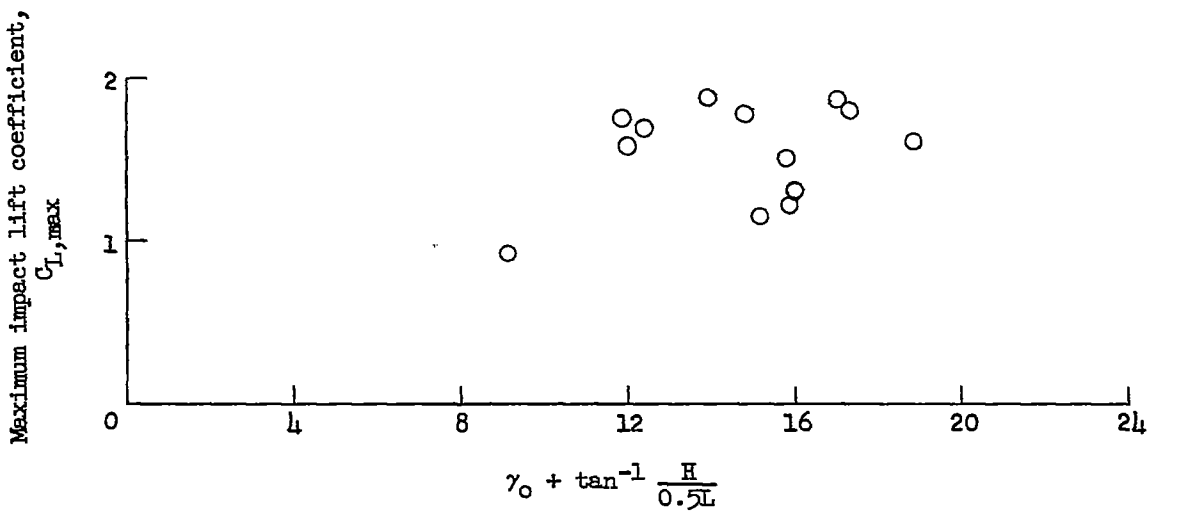

(b) Second impacts.

Figure 17.- Variation of maximum impact lift coefficient with approximation of effective flight-path angle, $\gamma_o + \tan^{-1}\frac{H}{0.5L}$.

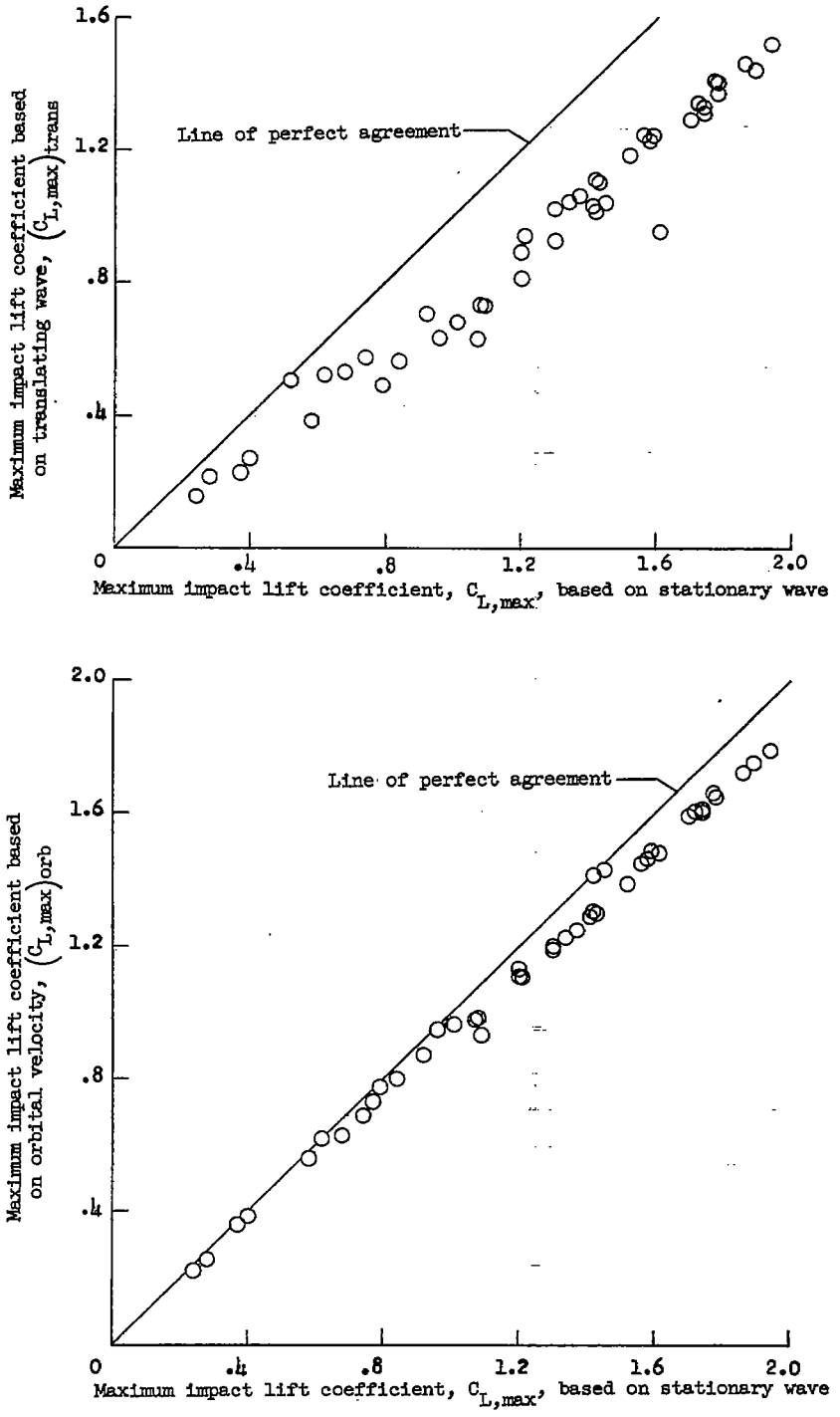

Figure 18.- Comparison of maximum impact lift coefficient for various methods of computation.